EFFECT OF THE TEST SET-UP ON FRACTURE MECHANICAL PARAMETERS OF CONCRETE

V. Mechtcherine and H.S. Müller,
Institute of Concrete Structures and Building Materials,
University of Karlsruhe, Germany

Abstract

In this investigation the effect of the test set-up on fracture mechanical parameters of concrete was studied experimentally and numerically. In the first step a series of deformation controlled uniaxial tension tests on dog-bone shaped specimens and notched specimens with rotatable and non-rotatable boundaries as well as three-point bend tests were performed. As a result, the experiments with rotatable loading platens provided lower values of the fracture energy G_F than the tests with non-rotatable boundaries, but slightly higher G_F-values than those obtained from the bend tests. In the second step, these experiments were analyzed numerically within the frame of a smeared crack concept. The analysis showed, that the G_F-values obtained from the uniaxial tension tests with non-rotatable loading platens are the most realistic ones.

Key words: Fracture energy, uniaxial tension, boundary rotatability, bending, numerical analysis, cohesive crack models

1 Introduction

Numerical modeling using the cohesive crack type models, within the frame of a discrete (e.g. Hillerborg et al. 1976) or a smeared (e.g. Bazant and Oh, 1983) crack approach, is one of the most suitable tools for solving various practical problems with regard to concrete failure and

fracture phenomena in concrete. Though these models are widely applied, there is still no clarity concerning experimental determination of their input parameter, especially of the fracture energy G_F. Recently, van Mier et al. (1996) investigated the influence of the boundary rotatability in uniaxial tension tests experimentally and numerically. They concluded that the tests with rotatable loading platens were more suitable because in those tests a lower limit for the fracture energy had been found. However, the lattice model used in their numerical simulations does not enable to prove the correctness of this conclusion.

The main purpose of this study is to investigate the effect of the test set-up on fracture mechanical parameters of concrete and to clarify, which values should be used as input parameters in corresponding numerical analyses.

2 Concrete composition, preparation of specimens and test set-up

The composition of the investigated concrete is given in Table 1. For the mixture ordinary Portland cement CEM I 32,5 R was used. As aggregate quartzite Rhine sand and gravel were applied. The compressive strength of the concrete obtained from the tests on cube specimens at an age of 28 days was 44 MPa.

Table 1. Composition of the concrete

w/c	Cement CEM I 32,5 R [kg/m^3]	Aggregate [kg/m^3]			Superplasticizer [kg/m^3]
		0-2 mm	2-8 mm	8-16 mm	
0.6	318	543	688	580	1

Dog-bone shaped prisms with a gauge length of 250 mm were chosen to determine the uniaxial tensile strength f_t and the tangent modulus of elasticity E_0 (see Fig. 1, left). Notched prisms were used to determine the fracture energy G_F and the complete stress-deformation relation (Fig. 1, middle). Both types of specimens had the same effective cross-section of 60×100 mm^2.

In addition three-point bend tests were performed. The beam specimens ($570\times100\times100$ mm^3) also had the effective cross-section of 60×100 mm^2. In the middle of the specimen with a span of 500 mm a 40 mm deep notch was sawn. A schematic view of the geometry of the specimens and a typical load-deflection relation are given in Fig. 1 (right). Details may be found in the thesis of Mechtcherine (1998).
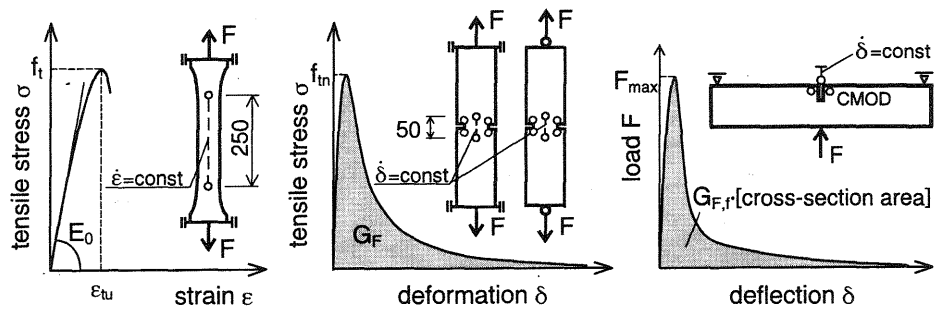
Fig. 1. Schematic view of the geometry of the 3 types of specimens used, and typical corresponding relations obtained from the tests (geometrical data in [mm])

All specimens were cast horizontally in metal forms. After demoulding, the specimens were wrapped in a thin plastic sheet to which an aluminium foil was glued in order to protect the concrete against desiccation. All specimens were tested at a concrete age of 56 days.

The uniaxial tension tests on the dog-bone shaped prisms were performed with non-rotatable boundaries. For this purpose, stiff metal adapters were glued to the specimens. Finally the metal adapters were firmly connected with the bearing platens of the testing machine. The experiments on the notched prisms were carried out both with non-rotatable and rotatable boundaries. For the set-up with rotatable boundaries hinges were built in between the metal adapters and the bearing platens.

In the tests on the dog-bone shaped prisms the strain rate was controlled by means of the average signal of two LVDTs fixed to the specimens. For the experiments on the notched prisms two LVDTs with a gauge length of 50 mm were placed in the middle of the notched cross-section to achieve a better deformation rate control. Four further LVDTs with a gauge length of 25 mm were placed on the notch tips on both sides of the specimen to measure local deformations (e.g. LVDTs 1 and 3 in Fig. 2).

The tensile tests on dog-bone shaped prisms were performed with the strain rate of $\dot{\varepsilon} = 10^{-5}$ 1/s. The corresponding deformation rate $\dot{\delta}$ in the tensile tests on notched specimens was $5 \cdot 10^{-4}$ mm/s.

In the three-point bend tests the load was applied from below in order to compensate the dead weight (Fig. 1, right). In these tests the deflection rate of $1.667 \cdot 10^{-3}$ mm/s was kept constant.

For each investigated parameter at least three specimens were tested.

3 Experimental results

The main results of the performed fracture mechanical experiments are shown in Table 2. The mean uniaxial tensile strength f_t of the investigated concrete determined on the dog-bone prisms is 4.2 MPa. The modulus of elasticity E_0 was found to be 37.1 MPa.

Fig. 2 shows typical load-local deformation curves obtained from the experiments on the notched prisms with different boundary conditions. In both cases the first crack develops on the right notch of the prisms (see the curves for LVDT 3 in Fig. 2). In the tests with rotatable loading platens the crack continues to propagate solely from the right side into the specimens, while in the test with non-rotatable boundaries also on the opposite side a new crack starts to grow. In this case, at a deformation δ of approximately 0.025 mm the crack opening becomes uniform for the entire cross-section.

The comparison of the mean curves for the deformations measured at the middle of the cross-section (Fig. 3) is of major interest, since these curves are used for the determination of the fracture energy of concrete. The fracture energy is defined as the energy per unit area needed for the complete separation of a specimen into two parts. This value corresponds to the area under the σ-δ-relation.

At small deformations ($\delta < 0.1$ mm) the σ-δ-relation obtained from tests with non-rotatable boundaries is above the corresponding relation for tests with rotatable loading platens (Fig. 3). As a result the tests with rotatable boundaries provide lower values of the net tensile strength f_{tn} and
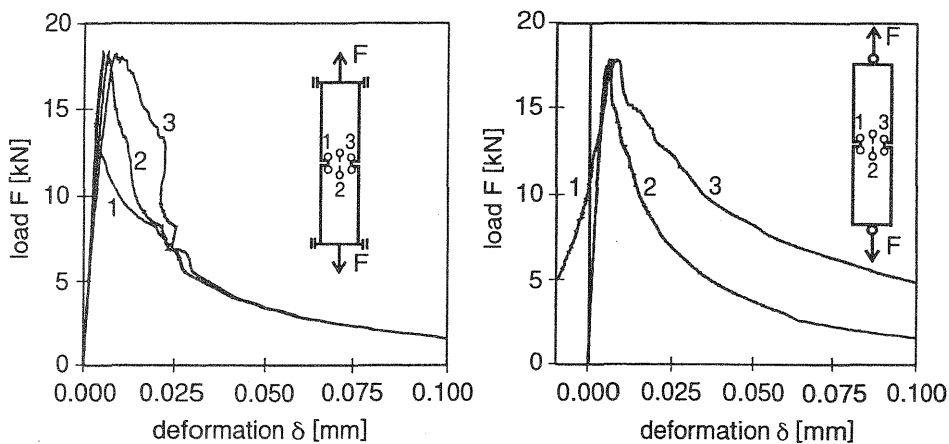

Fig. 2. Typical F-δ-relations obtained from uniaxial tension tests with non-rotatable (left) and rotatable loading platens (right)
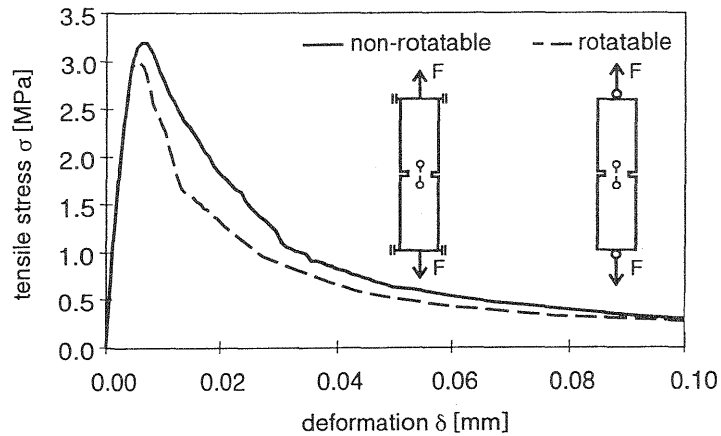
Fig. 3. Effect of the boundaries at testing on the shape of the σ-δ-relation

of the fracture energy G_F (see Table 2). Both values for the net tensile strength f_{tn} are lower than f_t, indicating a notch sensitivity of the concrete.

The most important results of the three-point bend tests are also presented in Table 2. The bending strength f_{ft} was calculated from the maximal load considering linear-elastic behaviour of the material. The specific fracture energy $G_{F,f}$ was determined as the ratio between the area under the load-deflection diagram and the effective cross-section. This value was found to be slightly lower than the fracture energy values obtained from the tension tests with rotatable boundaries.

Table 2. Results of the fracture mechanical experiments

Test	Rotatability	f_t [*] [MPa]	E_0 [GPa]	G_F [**] [N/m]
Tension, dog-bone prisms	non-rotatable	4.2 (0.1)	37.1 (0.7)	–
Tension, notched prisms	non-rotatable	3.2 (0.3)	–	130.1 (15.2)
	rotatable	3.0 (0.2)	–	119.4 (18.4)
Bending	–	5.0 (0.3)	–	115.1 (16.5)

* f_t corresponds to f_{tn} for the tensile tests on the notched prisms or to f_{ft} for the bend tests.
** G_F corresponds to $G_{F,f}$ for the bend tests.
Standard deviations are given in parentheses.

4 Numerical investigations

For the numerical analysis of the influence of the test set-up on the fracture mechanical behaviour of concrete using the FE method, the crack band model (Bazant and Oh, 1983) was chosen. This model is closely related to the fictitious crack model of Hillerborg et al. (1976) (see Fig. 4), and can be considered to be representative for the cohesive crack type models.
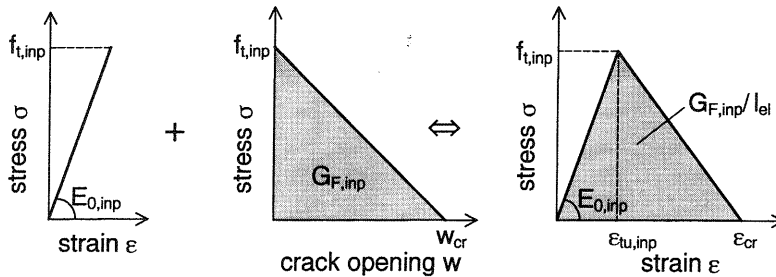

Fig. 4. Fictitious crack model (left) and the applied crack band model (right) for the description of behaviour of concrete subjected to tension

The tensile strength $f_{t,inp}$ (inp = input) and the modulus of elasticity $E_{0,inp}$ used for the model were taken directly from the experiments on the dog-bone shaped prisms (see Table 2). For better understanding of the results of the calculations a simple linear softening behaviour has been chosen. Accordingly, not the entire fracture energy G_F but only the energy $G_{F,inp}$ corresponding approximately the area under the first, steeper part of the descending branch of the σ-δ-relation measured in the uniaxial tension tests was taken. With the obtained value of $G_{F,inp} = 63$ N/m the corresponding critical crack opening $w_{cr} = 2 \cdot G_{F,inp}/f_{t,inp}$ was 0.3 mm.

The FE calculations were performed under the assumption of plane stress conditions. The areas of the test specimens where a crack may develop were modeled by quadratic elements with a side length l_{el} of 5 mm.

In the first series of simulations of the uniaxial tension tests exactly the same properties were assigned to all finite elements. Consequently, vertical and horizontal symmetries of the crack development were observed (Fig. 5), what is certainly not realistic. However, considering only one of the both failure bands in the simulation of the test on a dog-bone specimen (marked with arrows in Fig. 5), the calculated σ-δ-relation corresponds very well to the applied material law (see diagram in Fig. 5 as well as the ratios $f_{t,cal}/f_{t,inp}$ and $G_{F,cal}/G_{F,inp}$ in Table 3). In the numerical calculations considering a notched prism, similar to the tests, a notch sen-
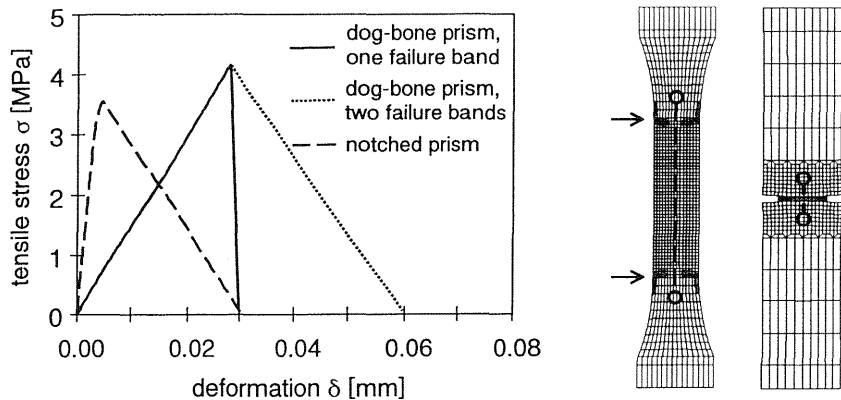
Fig. 5. Calculated σ-δ-relations and the distributions of the strains $\varepsilon > \varepsilon_{tu,inp}$ in the simulation of the tests where concrete is modeled as a homogeneous material (magnification factor for deformations = 500)

sitivity of the concrete was observed: the $f_{tn,cal}$- and $G_{Fn,cal}$-values were found to be smaller than the corresponding values $f_{t,cal}$ and $G_{F,cal}$ obtained from the simulation of the tests on the dog-bone prisms (Table 3).

As a result of the assumed homogeneity of concrete no effect of boundaries on the cracking behaviour could be observed in the simulations. However, concrete is actually a highly non-homogeneous material at this level of consideration. To consider the heterogeneity of concrete an imperfection was introduced into the model by the reduction of the tensile strength of just one finite element on the right notch by 20 %.

Fig. 6 shows the calculated stress-deformation relations and the corresponding distributions of strains ε exceeding the ultimate strain $\varepsilon_{tu,inp} = f_{t,inp}/E_{0,inp}$. In the case of rotatable boundaries, initial cracking occurs at the „weaker" notch and then the crack propagates across the ligament towards the opposite notch. As a result, more and more eccentricity is gradually introduced in the test set-up throughout the experiment (Fig. 6).

A different behaviour was predicted for the case of non-rotatable boundaries: the reduction of the stiffness at the cracked side through the first crack on the weaker notch and the non-rotatable boundaries lead to the development of the second crack at the opposite notch. From then on a rather symmetrical development of the both cracks as well as an almost uniform distribution of strains throughout the entire cross-section can be observed (Fig. 6).

For the both types of boundary conditions the calculated curves of stress versus local deformations exhibited qualitatively the same shapes as the measured σ-δ-relations (compare Fig. 6 and Fig. 2). The σ-δ-curve
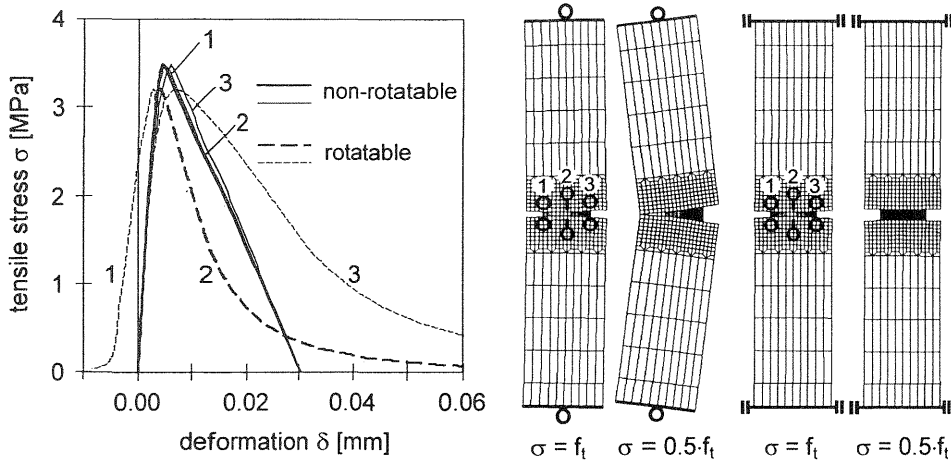
Fig. 6. Effect of the rotatability of the boundaries at tension tests on the shape of the calculated σ-δ-relations and the crack development in notched specimens (magnification factor for deformations = 500)

for the middle of the notched cross-section obtained from the simulation of the tests with rotatable boundaries showed, in contrast to the σ-δ-curve for the tests with non-rotatable boundaries, a highly non-linear shape for the descending branch, which differs very much from the shape of the applied material law (compare Fig. 6 and Fig. 4). Hereby, the numerically simulated tests with rotatable loading platens provided - in agreement with the experimental results - a lower tensile strength and fracture energy as the tests with non-rotatable boundaries (Table 3).

The simulation of the three-point bend tests was performed assuming concrete to be a perfect homogeneous material (Fig. 7). The calculated fracture energy $G_{Fn,cal}$ was found to be slightly lower than the corresponding value from the simulation of the tension tests with rotatable boundaries (Table 3).
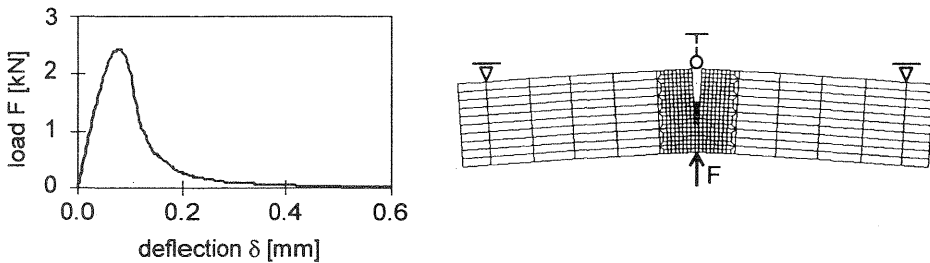

Fig. 7. Calculated F-δ-relation and the distributions of the strains $\varepsilon > \varepsilon_{tu,inp}$ in the bend test (magnification factor for deformations = 200)

384

Table 3. Results of the numerical simulations

Test	Rotatability Homogeneity	$f_{t,cal}$* [MPa]	$f_{t,cal}/f_{t,inp}$ [-]	$G_{F,cal}$* [N/m]	$G_{F,cal}/G_{F,inp}$ [-]
Tension, dog-bone prisms	non-rotatable homogeneous	4.17	0.99	63.1	1.00
Tension, notched prisms	non-rotatable homogeneous	3.56	0.85	55.8	0.89
	non-rotatable imperfection	3.50	0.83	54.6	0.87
	rotatable imperfection	3.21	0.76	47.9	0.76
Bending	homogeneous	5.08	1.58	46.8	0.74

* $f_{t,cal}$ or $G_{F,cal}$ correspond to $f_{tn,cal}$ or $G_{Fn,cal}$ for the tests on the notched prisms, and to $f_{ft,cal}$ or $G_{Ff,cal}$ for the bend tests, respectively.

5 Summary and conclusions

In this study the influence of the test set-up on fracture mechanical parameters of concrete was investigated. Herein, the experiments with rotatable boundaries provided lower values of the tensile strength f_{tn} and the fracture energy G_F than the tests with non-rotatable loading platens. The measured values of the fracture energy from the three-point bend tests were found to be slightly lower than the G_F–values obtained from the uniaxial tensile tests with rotatable loading platens.

Further, the tests were analyzed numerically using the crack band model. The results obtained from these simulations were compared with the experimental findings and with the input parameters of the numerical model. There, the main evaluation criterion resulted from the consideration, how well the calculated response of the model matches the applied material law.

The calculated response of the dog-bone prisms loaded in uniaxial tension showed nearly a perfect correspondence with the applied material law. The numerically simulated tests on the notched specimens with non-rotatable boundaries provided lower values of the tensile strength and the fracture energy as the corresponding input values. However, the calculated softening behaviour complied rather well with the softening formulation of the material law. In contrast to that, the computation of the tests with rotatable boundaries resulted in a stress-deformation

relation, which was, concerning its shape, very different from the input material law. The results of the numerical simulations concerning the tensile strength, the bending strength as well as the fracture energy were found to be in a good agreement with the experimental findings.

The results summarized above allow to draw the following conclusions with regard to the determination of the input parameters for numerical analyses using cohesive crack type models:

- The tensile strength f_t and the modulus of elasticity E_0 for the material law should be determined from uniaxial tension tests on unnotched specimens with non-rotatable boundaries.

- In ideal case, also the fracture energy G_F and the shape of the softening curve should be obtained from such tests. However, it is much easier to perform stable experiments on notched specimens. Hereby, uniaxial tension tests with non-rotatable boundaries provide a descending branch of the σ-δ-relation, which shows the best correspondence with the real softening behaviour of concrete.

- When deriving a stress-crack opening relation from the σ-δ-relations obtained in tests with non-rotatable boundaries its first, steeper part should be corrected upwards to mach the tensile strength f_t. As a result, also the value of the input fracture energy increases up to the correct value. The second, shallow part of the softening branch can be taken over directly from the measured σ-δ-relations.

6 References

Bazant, Z.P. and Oh, B.H. (1983) Crack band theory for fracture of concrete. **Materials and Structures**, 16, 155-177.

Hillerborg, A., Modéer, M. and Petersson, P.E. (1976) Analysis of crack formation and crack growth in concrete by means of fracture mechanics and finite elements. **Cement & Concrete Research**, 6, 773-782.

Mechtcherine, V. (1998) **Fracture mechanical, fractological and numerical investigations on concretes**. Doctoral thesis (in German), Institute of Concrete Structures and Building Materials, University of Karlsruhe (in preparation).

Van Mier, J.G.M., Schlangen, E. and Vervuurt, A. (1996) Tensile cracking in concrete and sandstone: Part 2 - Effect of boundary rotations. **Materials and Structures**, 29, 87-96.